IIETA International Information and Engineering Technology Association
Advancing the World of Information and Engineering

Mathematical Modelling of Engineering Problems
Vol. 12, No. 12, December, 2025, pp. 4141-4150
Journal homepage: http://iieta.org/journals/mmep

Effect of Lime and Fly Ash Soil Treatment on Pore Water Pressure Response in Earth Dams under Rapid Drawdown

Ali M. Madhloom[1*], Abdulaziz A. Al-Kifae[1], Saleh I. Khassaf[2]

[1] Civil Engineering Department, Al-Nahrain University, Baghdad 10070, Iraq
[2] Civil Engineering Department, University of Basrah, Basrah 61001, Iraq

Corresponding Author Email: ali.muzher@buog.edu.iq

https://doi.org/10.18280/mmep.121204

Received: 18 September 2025
Revised: 23 November 2025
Accepted: 28 November 2025
Available online: 31 December 2025

Keywords:
permeability, rapid drawdown, pore water pressure, seepage, earth dam, lime-fly ash additives

ABSTRACT

Rapid drawdown is one of the most critical conditions in a dam's lifespan, as sudden reservoir drainage induces pore pressure imbalances that may threaten upstream slope stability. Therefore, ensuring slope stability through proper design remains a key safety consideration. This study investigates how variations in permeability affect the pore water pressure response in treated earth dams subjected to rapid drawdown. A physical model of an earth dam was constructed, with core soil was treated with varying lime–fly ash ratios (M-1 to M-4) and compared to an untreated control. Rapid drawdown was simulated by reducing the upstream water level from 36 cm to 5 cm within 5 min, while pore water pressures were monitored using ten sensors distributed across the dam section. Results indicate that the untreated control model exhibited rapid pore pressure dissipation due to high core and shell permeability. In contrast, treated models showed delayed dissipation, proportional to the additive content, with M-4 presenting the slowest response and most significant pressure dissipation delay. Nonetheless, the high-permeability shell zone effectively mitigated adverse effects on upstream slope stability. Numerical validation demonstrated excellent agreement with experimental data (coefficient of determination, $R^2 > 0.95$). Seepage analysis further confirmed that seepage towards the downstream direction decreased progressively with treatment, while exit gradients were effectively reduced to zero on the downstream slope at higher treatment levels.

1. INTRODUCTION

Rapid drawdown refers to a sudden and substantial decrease in the water level at the upstream face of an earth dam. This condition may occur due to operational needs, emergency discharges, or flood control. During rapid drawdown, the upstream slope of the dam is subjected to a loss of water pressure support while internal pore pressures within the dam remain elevated, depending on the permeability of the dam material [1]. This imbalance can lead to slope instability and structural failure if not properly analyzed and mitigated during the design process [2].

Assessment of the stability of earth dams under rapid drawdown is essential, particularly for dams with low-permeability materials, where pore pressure dissipation is slow [3]. Consequently, a key factor influencing stability under rapid drawdown is the soil's ability to dissipate pore pressure. This ability is largely determined by the permeability of the dam material. Low-permeability soils require more time to reach equilibrium between internal pore pressure heads and the external water level compared to more permeable soils [4]. Evaluation of the distribution of pore water pressures during drawdown is therefore a critical aspect in evaluating stability [5].

Recent studies emphasize the strong relationship between soil permeability and the rate of pore pressure dissipation during rapid drawdown. Ahmed [6] demonstrated that rapid drawdown produces steep hydraulic gradients and delayed dissipation of pore pressures, particularly in low-permeability zones, leading to significant reductions in the factor of safety. Similarly, Noori and Salim [7] showed that decreasing the shell permeability directly slows pore pressure dissipation and significantly reduces upstream slope stability under rapid drawdown. Similar conclusions were reached by Pandey et al. [8], who found that excess pore pressure within low-permeability dam shells is a primary cause of instability during rapid reservoir lowering, and that increasing shell permeability or adopting filtration measures enhances stability performance.

A rapid drawdown of reservoir water levels induces a steep hydraulic gradient between the upstream shell of the dam and the adjacent reservoir. This condition accelerates the seepage rate through both the upstream face and the foundation in the upstream zone. When the hydraulic gradient approaches its critical value, the average seepage force becomes equal to the submerged soil weight, thereby reducing the effective stress at that point to zero [9]. Under these conditions, the erosive potential of the soil progressively increases until concentrated seepage develops at the exit points. The emergence of seepage on the upstream slope following drawdown has a significant

impact on stability, as it not only reduces effective stress through elevated pore pressures but also increases the destabilizing forces within the soil mass due to additional seepage pressures [10]. Consequently, the combined effects of excess pore pressures and seepage-induced driving forces can substantially reduce upstream slope stability [11].

The impact of reservoir drawdown on the stability of slopes and earth dams has been examined from multiple viewpoints. Experimental studies have demonstrated the hydraulic and geotechnical responses of soils under drawdown scenarios [12, 13]. In contrast, numerical modeling has provided a valuable understanding of transient seepage behavior and associated stability concerns [14-16]. While, limit equilibrium and analytical methods have been employed to assess slope safety during rapid water level changes [17-19].

Many studies have focused on improving the soil of earth dams, with most reporting favorable outcomes in reducing permeability and enhancing resistance to seepage [20, 21]. Shuhaib and Khassaf [22] examined the use of tire rubber powder (TRP) for improving earth-dam cores and found that higher TRP contents were more effective in reducing seepage. Several researchers have examined the use of lime and fly ash to improve the geotechnical and hydraulic properties of soils [23-25]. Husein and Chemeda [26] used lime additives to modify some of the unwanted properties of clayey soils, which are utilized to build the core of zoned earth dams, where the addition of 6% lime significantly decreased soil permeability from 4.47×10^{-6} to 3.63×10^{-7} m/s. According to Islam et al. [27], fly ash demonstrates greater effectiveness than lime in reducing the permeability of clayey and sandy soils in the range of 5–30%. Swamynaidu and Tyagi [28] investigated the hydraulic conductivity of fly ash–cement–alkali-activated (FCAA) clay mixes for use as low-permeability hydraulic barriers. The results indicated that FCAA-treated clays exhibited lower or comparable hydraulic conductivity when compared with untreated clay.

While such improvements are generally beneficial for reducing permeability, controlling seepage, and increasing structural integrity under steady-state conditions, a critical aspect that is often overlooked is the potential drawback under rapid drawdown conditions. Specifically, reducing the permeability of the dam's soil can hinder the dissipation of excess pore pressures, resulting in a delayed hydraulic response. This delay in pressure dissipation may increase the risk of instability along the upstream slope, highlighting the importance of evaluating soil treatment methods not only for seepage control under steady-state conditions but also for their performance during sudden reservoir drawdown. The significance of this study lies in its dual evaluation; while examining the effectiveness of lime–fly ash treatment in reducing seepage and improving core impermeability, it also addresses the potential challenges posed by slower pore pressure dissipation in treated soils. The outcomes offer practical guidance for designers, ensuring an optimal balance between seepage reduction and drawdown stability. Addressing this knowledge gap could facilitate the development of more effective and comprehensive strategies for controlling seepage under rapid drawdown conditions, thereby improving safety and supporting sustainable infrastructure.

In this research, an experimental study was carried out to investigate the effect of changes in permeability on the hydraulic and stability behavior of treated earth dam models subjected to rapid drawdown. Sandy soil was treated with varying percentages of lime and fly ash additives and used in the core zone of four experimental dam models (M-1, M-2, M-3, and M-4), while an untreated control model was constructed for comparison. Laboratory-scale physical models were subjected to controlled rapid drawdown conditions, in which the upstream water level was reduced from 36 cm to 5 cm within a duration of 5 min. Pore water pressure responses were continuously monitored using ten pressure sensors.

2. MATERIALS AND METHODS

2.1 Experimental model design

A rectangular basin containing an earth dam model was constructed as the experimental model (Figure 1). This apparatus was specifically designed to study seepage behavior in permeable media. It also allowed for the evaluation of changes in seepage rate and phreatic surface position resulting from the treatment of the earth dam with different additive proportions.

The cross-sectional dimensions of the physical model were not chosen arbitrarily; all design criteria were considered when determining the final size. The top width, freeboard, upstream and downstream slopes, maximum water level, and all other requirements were established based on suggestions and recommendations [29]. Following that, the dam geometry was scaled down to produce a model suitable for the basin. This scaling ensured practical model dimensions, allowing for controlled seepage monitoring within the laboratory facility.

The earth dam model was positioned at the center of the basin. It had overall dimensions of 170 cm in length, 18 cm in width, and 40 cm in height. Based on the characteristics of the soil, both the upstream and downstream slopes were constructed with an inclination of 1:2 (vertical: horizontal). A maximum reservoir water depth of 36 cm was adopted and maintained consistently throughout all experimental cases in this study.

The basin itself measured 210 cm in length, 50 cm in height, and 18 cm in width, and was fabricated using transparent Plexiglas panels with a thickness of 1 cm.

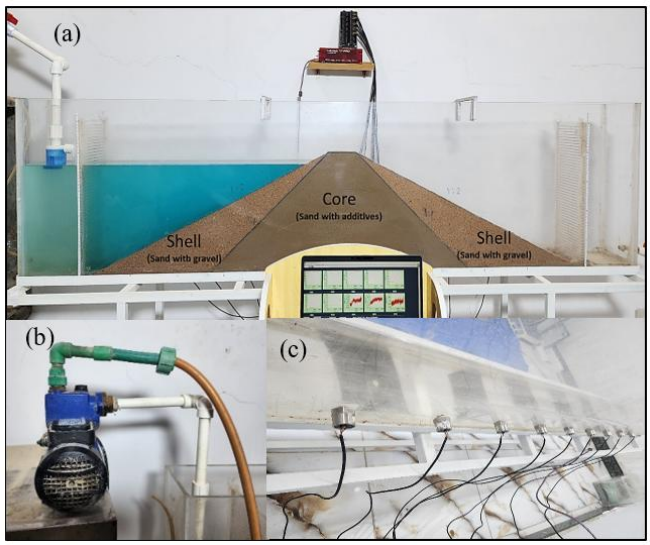

Figure 1. Schematic diagram of the experimental setup: (a) Plexiglas basin and an earth dam model, (b) The water pump, (c) Pressure sensors

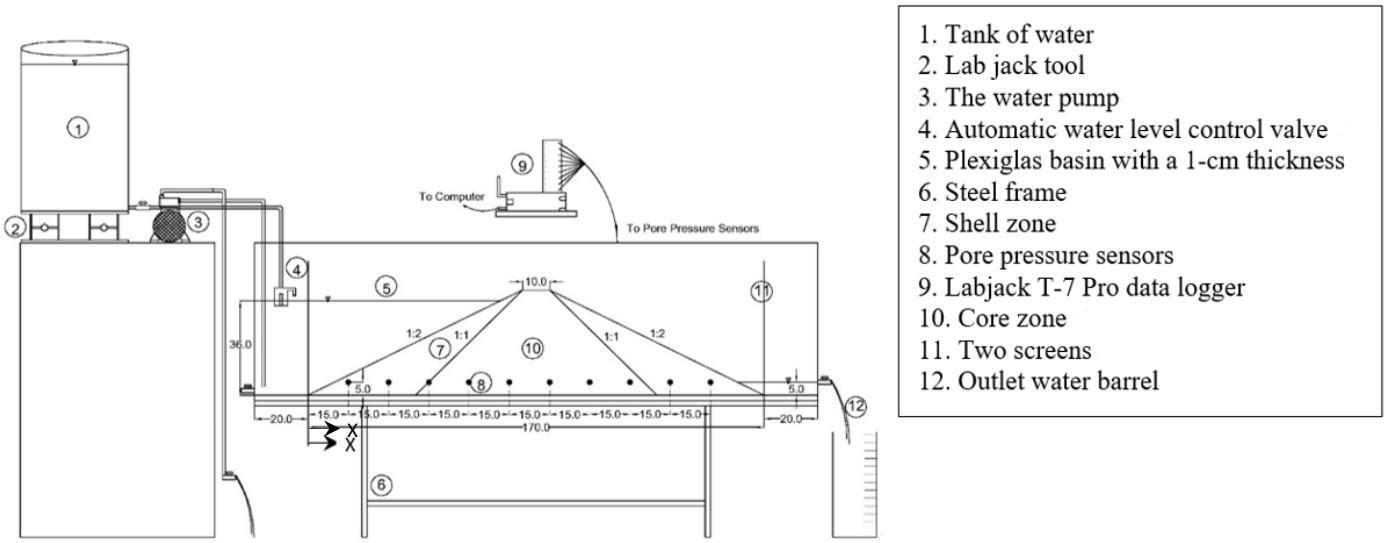

Figure 2. Experimental model layout of the earth dam (all dimensions in cm)

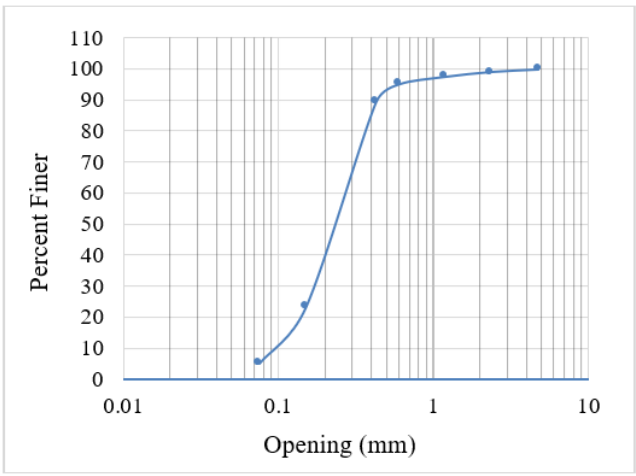

Figure 3. Grain size distribution curve of sandy soil

As illustrated in Figure 2, the experimental basin was mounted on a steel frame elevated 50 cm above ground level and carefully leveled in all directions. To protect the Plexiglas base from damage and to reduce vibrations generated during soil compaction, thin rubber sheets were installed along the basin floor. All joints were sealed using a waterproof sealing adhesive to prevent leakage.

Openings for the pressure sensors were precisely fabricated using a laser-cutting technique. These openings were located 5 cm above the basin base and arranged at horizontal distances of 0.15, 0.30, 0.45, 0.60, 0.75, 0.90, 1.05, 1.20, 1.35, and 1.50 m from the upstream toe.

A raised water supply tank was installed on the upstream side of the basin. The tank, with a total capacity of 81.5 liters, was used to fill the reservoir of the earth dam model. It was connected to the basin through a plastic pipe equipped with an automatic float valve, which ensured that the maximum water level remained constant throughout the testing period. The valve operates by automatically shutting off the inflow when the water surface reaches the preset elevation and resuming the supply once the level drops. The elevation of the float valve was controlled using a jack installed beneath the tank.

To simulate real rapid drawdown conditions, a controlled water pump was used to discharge water from the upstream side. Variations in seepage rate were monitored by drilling a hole in the lower portion of the earth dam and connecting it to the graded water barrel on the model's right side.

The earth dam model was constructed in eight successive layers, each measuring 5 cm in thickness after compaction. The required soil quantity for each layer was determined by calculating the soil dry density at 90% compaction, based on its maximum dry density and the dam's geometric dimensions. Compaction was performed using a standard square hammer, achieving the target density in each layer at the optimal moisture content.

To monitor the phreatic surface within the dam, ten pressure sensors were installed and connected to a data logger, recording readings every five seconds to identify the final phreatic surface location. In the physical model, the basin bed acted as an impervious layer, ensuring that all seepage occurred through the dam body only.

2.2 Soil of the dam body

The experimental investigations were conducted using two locally sourced soils. The first soil consisted of sand with gravel, representing the material used in the shell of an earth dam. The second soil was sandy and was improved with various additives to simulate the material in the dam's core zone.

Figure 3 presents the particle size distribution curve for the sandy soil designated for the core. Since 5.2% of the particles pass through a No. 200 sieve, the soil is classified as A-3 (fine sand) according to the AASHTO classification system and as SP (poorly graded sand) under the Unified Soil Classification System (USCS).

2.3 Lime and fly ash additives

Two types of additives, lime and fly ash, were used to improve the characteristics of the soil in the core construction. In this investigation, hydrated lime was obtained from the Karbala Lime Factory, which manufactured it in compliance with Iraqi Standard No. 807/2004 [30]. The chemical analysis of the lime used is displayed in Table 1.

According to the chemical analysis of fly ash obtained from laboratory testing, which is displayed in Table 2, the fly ash's chemical composition conforms to ASTM C-618 [31] requirements.

Table 1. Chemical analysis of hydrated lime [%]

Composition	[%]
Silica (SiO_2)	3.26
Alumina (Al_2O_3)	0.67
Ferric oxide (Fe_2O_3)	0.22
Magnesium oxide (MgO)	0.3
Calcium oxide (Cao)	69.72
Sulfur trioxide (SO_3)	0.28
Sodium oxide (Na_2O)	0.15
L.O.I	25.6

Table 2. Chemical analysis of fly ash measured by XRF

Composition	[%]
Silica (SiO_2)	58.34
Alumina (Al_2O_3)	26.62
Ferric oxide (Fe_2O_3)	3.19
Magnesium oxide (MgO)	2.88
Calcium oxide (Cao)	2.44
Sulfur trioxide (SO_3)	0.15
Sodium oxide (Na_2O)	0.65
L.O.I	2.8

Table 3. Codes of the different models being studied

Lime + Fly Ash (% by Weight)	Model Code
0	Control model
3% Lime + 9% Fly ash	M-1
5% Lime + 15% Fly ash	M-2
7% Lime + 21% Fly ash	M-3
9% Lime + 27% Fly ash	M-4

Table 4. Summary of permeability (k) for sandy soil after a saturation period of 48 hours

Soil Type	Lime + Fly Ash (% by Weight)	The Permeability (m/s)
Shell soil (sand with gravel)	0	3.98×10^{-4}
Core soil (sand)	0	8.17×10^{-5}
	3% Lime + 9% Fly ash	4.962×10^{-6}
	5% Lime + 15% Fly ash	1.19×10^{-6}
	7% Lime + 21% Fly ash	7.71×10^{-7}
	9% Lime + 27% Fly ash	3.125×10^{-7}

2.4 Soil mixing with additives

In the core zone, sandy soil was combined with four percentages of lime-fly ash additives. These percentages, measured by weight, were: 3% Lime + 9% Fly ash, 5% Lime + 15% Fly ash, 7% Lime + 21% Fly ash, and 9% Lime + 27% Fly ash. As a result, many models were developed for the research, and these models were assigned codes, which are displayed in Table 3. These values were chosen in accordance with proportions recommended in the literature [32-35].

The permeability of the soil samples was determined using two standard laboratory methods: the constant head test and the falling head test, performed in accordance with ASTM D-2434 and ASTM D-5084 [36, 37]. For each test, the samples were compacted in layers to 90% of the maximum dry density at the optimum moisture content. When calculating the weight of soil for each layer, both the soil dry density and the cylinder volume used in the permeability test were considered. The experiments were conducted 48 hours after placing the samples in the test cell to ensure full saturation, allowing water to completely fill the soil voids, eliminate air bubbles, and achieve a steady-state seepage. The summarized results of these tests are presented in Table 4.

3. RESULTS AND DISCUSSION

3.1 Experimental results

To simulate real rapid drawdown conditions, a water pump was used to discharge water from the upstream side, as illustrated in Figure 2.

In this testing, a rate of rapid drawdown condition was simulated to assess the pore water pressure in the untreated control model and treated models (M-1, M-2, M-3, and M-4). The upstream water level was lowered from 36 cm to 5 cm over a period of 5 min using a controlled discharge pump. This scenario reflects realistic operational drawdown rates that may occur during reservoir lowering. Monitoring the internal pore pressures under this condition allowed for assessment of the hydraulic behavior of the dam body when the rate of drawdown provided limited time for pore pressure dissipation, especially in models with lower-permeability cores.

3.1.1 The control model

The control model serves as the reference for evaluating the behavior of pore water pressure under rapid drawdown. In this model, no modifications to the core's permeability were introduced. Before conducting the rapid drawdown, the model was filled and allowed to reach a steady-state seepage condition. Then, the water level on the upstream side was reduced from 36 cm to 5 cm within 5 min, simulating a rapid drawdown.

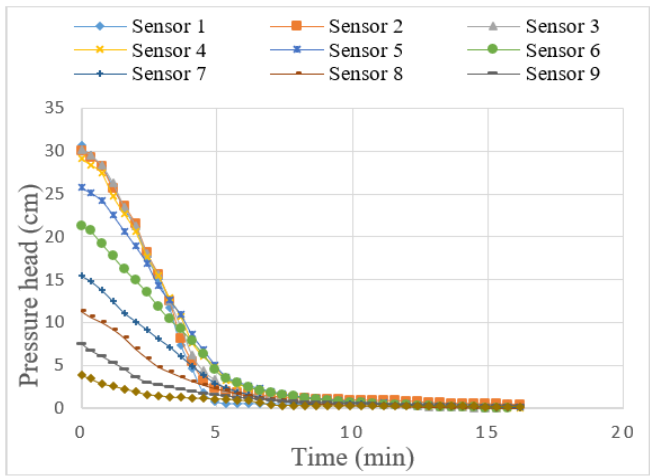

Figure 4. Monitoring of pressure head in the control model during rapid drawdown using ten sensors

As seen in Figure 4, the curves showed a steep decline in pressure head during the first 5 min of the drawdown process, indicating a rapid response of the steady-phreatic surface to the sudden change in the upstream water level. As time progressed beyond the 8 min mark, pressure head readings across all sensors stabilized, suggesting that the model was approaching a new equilibrium. The early decline of pressure head indicated fast pore pressure dissipation due to high permeability in the core and shell zones of the control model. However, the pore pressure sensor data indicated that achieving a new equilibrium between the external water level

and the internal pressure heads involved a slight delay in pressure dissipation, particularly noticeable at the 5 min mark, especially in the regions monitored by sensors 4, 5, and 6. The observed delay at these sensor locations compared to the external water level after the 5 min was 3.2 cm, 3.6 cm, and 3.4 cm, respectively (Figure 5).

3.1.2 The M-1 treated model

In model M-1, by around 20 min, the pressure head stabilized, with most sensors reaching near-steady conditions. This indicated that, despite the treatment applied in M-1, the pressure head still dissipated relatively quickly (Figure 6), reducing the duration of excess pore pressure and, consequently, the risk of instability.

The phreatic surface over time across the M-1 model is shown in Figure 7. At 0 min, the phreatic surface was high, corresponding to the initial steady-state condition. As the drawdown progressed, a distinct lowering of the phreatic surface was observed. Beyond 20 min, the phreatic surface flattened significantly, indicating that a new equilibrium condition was nearly achieved. The results indicated a slight delay in pore pressure dissipation within the M-1 model, particularly evident at the 5 min interval as the system approached a new equilibrium, indicating that internal pressure heads lagged behind the rapidly falling external water level. This delay was most noticeable at sensors 4, 5, and 6, with differences of 5.3 cm, 6.2 cm, and 5.4 cm, respectively.

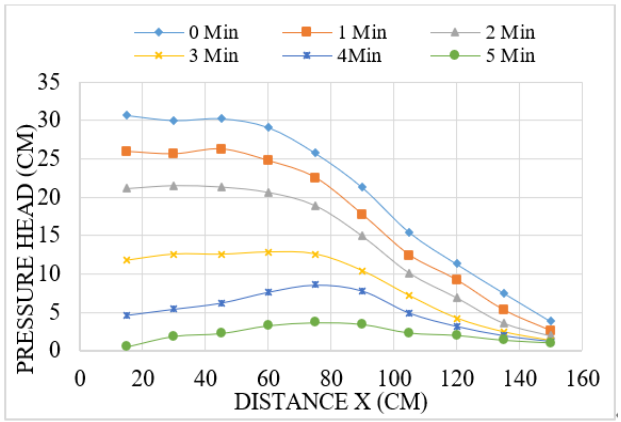

Figure 5. Evolution of the phreatic surface over time in the control model under rapid drawdown conditions

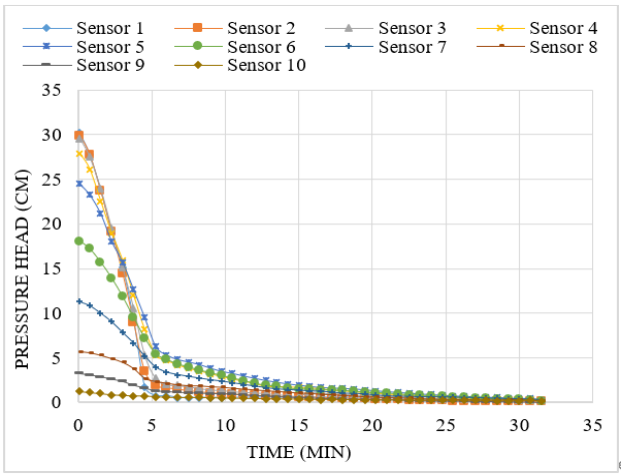

Figure 6. Monitoring of pressure head in the M-1 model during rapid drawdown using ten sensors

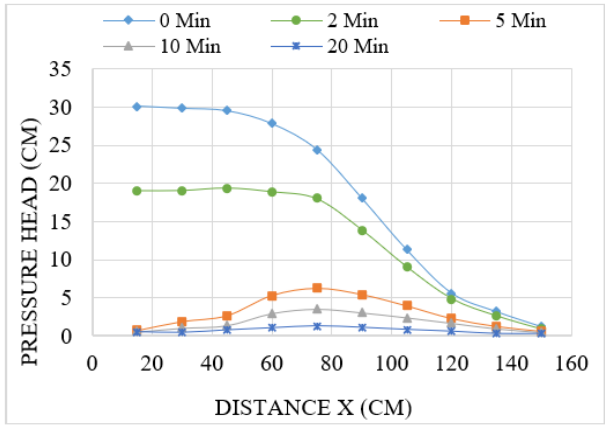

Figure 7. Evolution of the phreatic surface over time in the M-1 model under rapid drawdown conditions

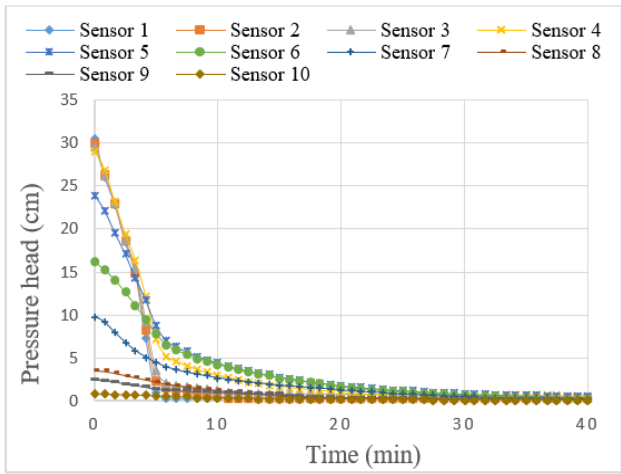

Figure 8. Monitoring of pressure head in the M-2 model during rapid drawdown using ten sensors

3.1.3 The M-2 treated model

Results of the pressure head in the M-2 model indicated a prompt response of the pore water pressures to the external drawdown (Figure 8). However, the magnitude and rate of dissipation were slightly slower than those in the M-1 model, suggesting a moderate reduction in permeability resulting from soil treatment. The pressure readings across all sensors continued to decline gradually thereafter, stabilizing around the 25 min mark.

At the 5 min mark, a clear delay was observed between the external water level and the internal pressure heads, particularly at sensors 4, 5, and 6 (Figure 9). This delay indicated a lag in internal pressure dissipation, attributed to the reduced permeability of the modified core material. The measured deviations at these sensor locations from the external water level were 7.2 cm, 8.8 cm, and 7.7 cm, respectively.

3.1.4 The M-3 treated model

Model M-3 (Figure 10) showed a slower and more gradual decline in pressure head, especially at sensors 4, 5, and 6, which began to diverge noticeably from the other sensors after the 5 min mark, characterized by a more gradual decline in pressure head. This behavior reflected the influence of reduced permeability resulting from the treatment applied in the M-3 core. Pressure equilibrium was reached after approximately 35

min, which delayed the establishment of final equilibrium but offered improved control of steady-state seepage.

At the 5 min mark, a significant delay was observed between the external water level and the internal pressure heads at sensors 4, 5, and 6 (Figure 11). This delayed pore pressure dissipation indicated the reduced permeability of the treated core material. The measured differences between the external water level and the pressure head at these sensor locations were 11.9 cm, 12.7 cm, and 9.6 cm, respectively.

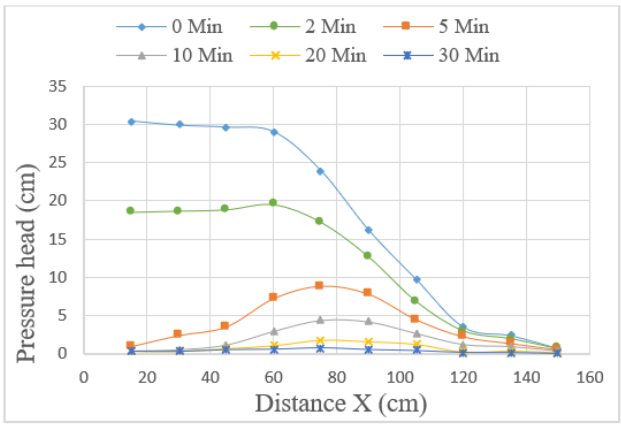

Figure 9. Evolution of the phreatic surface over time in the M-2 model under rapid drawdown conditions

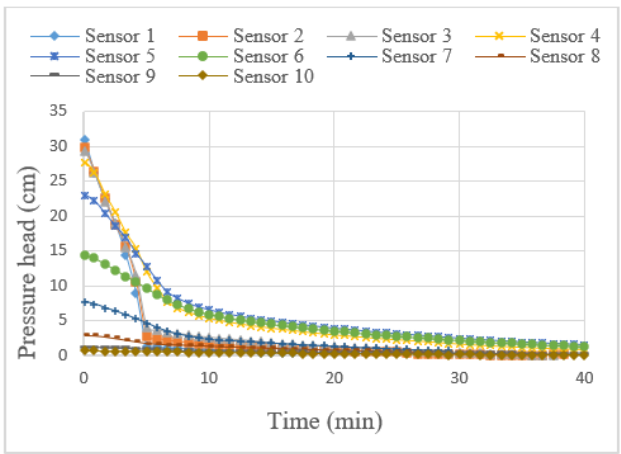

Figure 10. Monitoring of pressure head in the M-3 model during rapid drawdown using ten sensors

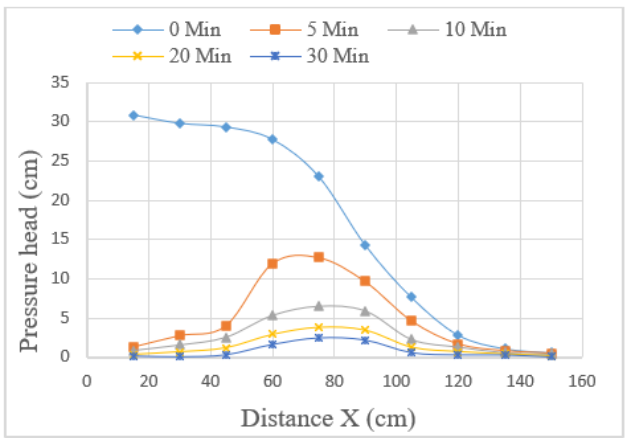

Figure 11. Evolution of the phreatic surface over time in the M-3 model under rapid drawdown conditions

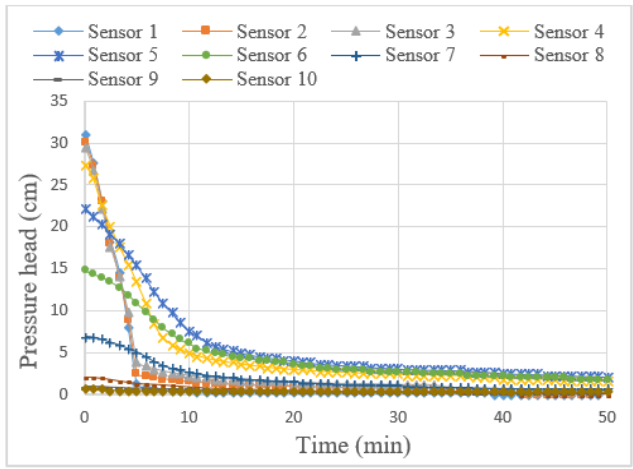

Figure 12. Monitoring of pressure head in the M-4 model during rapid drawdown using ten sensors

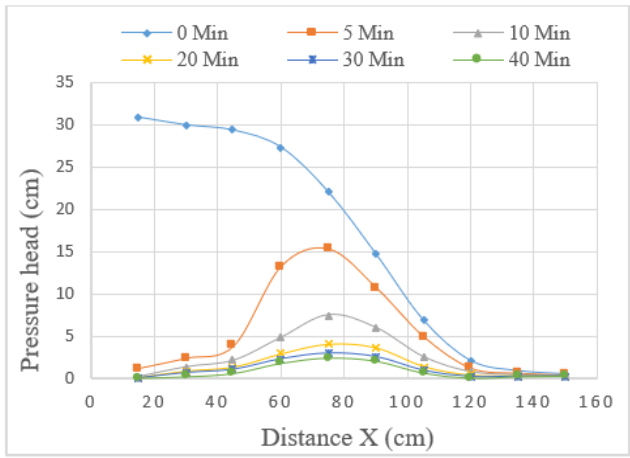

Figure 13. Evolution of the phreatic surface over time in the M-4 model under rapid drawdown conditions

3.1.5 The M-4 treated model

Model M-4 (Figure 12) demonstrated the slowest pore pressure dissipation among the three treated models, with stabilization of pressure head taking up to 45 min. The extended duration required to reach equilibrium suggested a treatment that significantly reduced the permeability of the core zone, creating zones of high pore pressure under drawdown. Although such treatment may have improved certain physical properties (e.g., strength or permeability), it also increased susceptibility to hydraulic instability due to delayed pressure equalization during rapid drawdown.

At the 5 min mark, a significant delay was observed between the external water level and the internal pressure heads at sensors 4, 5, and 6, positioned within the core zone (Figure 13). The recorded differences at these sensors were 13.3 cm, 15.4 cm, and 10.8 cm, respectively.

3.1.6 Summary of rapid drawdown in dam models

In the control model, pressure head stabilized shortly after 8 min, indicating rapid pore pressure dissipation. This behavior reflected the high permeability of the core and shell zones. In contrast, the treated models M-1, M-3, and M-4 demonstrated varying pore pressure dissipation behaviors under rapid drawdown conditions (36 cm to 5 cm in 5 min), primarily influenced by the reduction in permeability resulting

from the applied treatments.

In Models M-1 and M-2, although permeability was reduced, pressure head still dissipated relatively quickly, with most sensors stabilizing within about 20 and 25 min, respectively, indicating a moderate reduction in permeability. In contrast, Model M-3 showed a slower decline in pressure head, with equilibrium reached after approximately 35 min, reflecting a greater reduction in permeability that impeded the flow of water and delayed pressure equalization. Model M-4 exhibited the slowest pressure dissipation, with stabilization occurring after nearly 45 min, confirming that this model had the most significant permeability reduction.

The delayed dissipation of pore water pressure observed in the treated models highlighted the effect of reduced permeability in limiting water movement, extending the transient phase, and potentially maintaining excess pore pressures, which were critical factors in evaluating the stability of earth dams under rapid drawdown. However, in the treated models, a pore pressure dissipation within the shell zone occurred more rapidly, which enhanced the stability of the upstream slope. This behavior indicated that the high permeability of the shell zone mitigated the adverse effects of delayed pore pressure dissipation in the core zone, thereby ensuring that upstream slope stability was not significantly compromised.

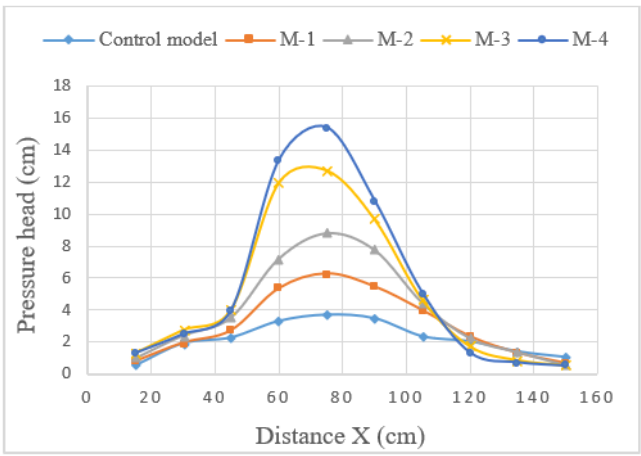

Figure 14. Phreatic surface comparison of control and treated models (M-1 to M-4) at the 5 min stage of rapid drawdown

Figure 15. Upstream slope of the M-4 model after rapid drawdown

In all models, the first 5 min marked the most critical condition during rapid drawdown, as there was a clear delay between the external upstream water level and the internal pore pressure heads (Figure 14). This delay indicated a state of hydraulic disequilibrium, where the rapid external drawdown had not yet been matched by internal pressure dissipation, increasing the risk of instability.

The control model exhibited the lowest pressure head, suggesting faster dissipation of pore pressure due to higher permeability. In contrast, treated models showed elevated pressure heads, particularly in the core zone, where the difference was most pronounced. Among the treated models, M-4 displayed the highest internal pressure, followed by M-3, M-2, and M-1.

Although M-4 provided the lowest seepage in steady-state conditions, its excessive permeability reduction caused a longer pore-pressure dissipation delay during rapid drawdown, which could temporarily increase susceptibility to hydraulic instability. This emphasized that overly low permeability might delay pressure equalization during rapid drawdown conditions, even if long-term seepage control improved (Figure 15).

3.2 Validation of the models

The numerical model was built using Slide 6.0 software. It incorporated the same geometry, material properties, and boundary conditions as the physical model to ensure comparability. Slide 6.0 used the governing equation in the partial differential form of Darcy's law, which was applied to predict the phreatic surface within the earth dam and to estimate seepage rates.

Governing equations for seepage flow were solved using finite element analysis. The finite element mesh used in this analysis is shown in Figure 16. The numerical query points and experimental sensors were positioned identically, 5 cm above the dam base and spaced at regular intervals from the upstream toe, ensuring a precise basis for comparison.

As shown in Figure 17, the numerical simulations across all models reproduced the overall shape and magnitude of the experimental phreatic surface, with only minor deviations observed in peak values, particularly within the central core zone where treatment effects were more pronounced. The determination coefficients (R^2) above 0.95 confirmed an excellent correlation, indicating that the numerical model accurately captured the seepage behavior and pressure distribution.

After validating the numerical model, the seepage rates and exit gradients of the control and treated models (M-1 to M-4) at 5 min of rapid drawdown were computed (Table 5). The upstream exit gradient was modest (~0.15–0.18), as the high-permeability shell zone allowed effective pore pressure dissipation. In contrast, the downstream exit gradient decreased from 0.10 to 0.00 as the level of treatment increased. Upstream seepage remained within a narrow range (8.96×10^{-5} to 1.03×10^{-4} m³/min), while downstream seepage decreased consistently from 8.49×10^{-5} m³/min in the control model to 2.34×10^{-5} m³/min in M-4. This behavior was linked to the initial steady-state condition, where upstream pressure heads at query points 1–4 were relatively similar across all models, while the reduced core permeability led to more pronounced differences in internal pressure head on the downstream side, thereby amplifying the decline in downstream seepage with increasing treatment level.

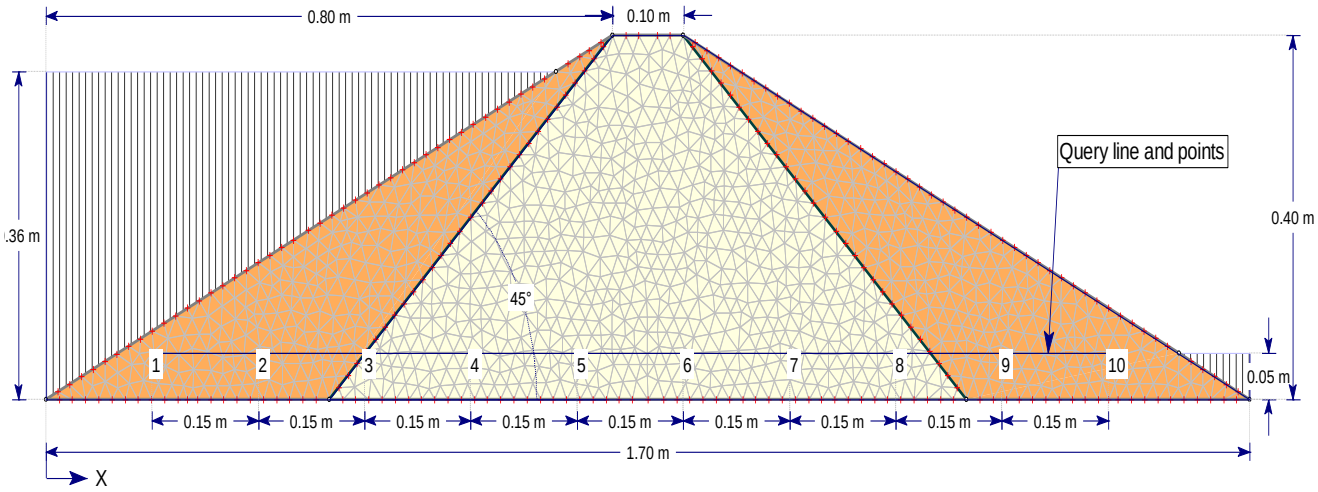

Figure 16. Cross-section of numerical earth dam model by program (slide 6.0)

Table 5. Seepage rates and exit gradients of the control and treated models (M-1 to M-4) at the 5-minute stage of rapid drawdown

Model Code	Seepage Rate (m^3/min)		Maximum Exit Gradient	
	Upstream Side	Downstream Side	Upstream Slope	Downstream Slope
Control model	8.96×10^{-5}	8.49×10^{-5}	0.15	0.1
M-1	1×10^{-4}	5.76×10^{-5}	0.16	0.07
M-2	1.03×10^{-4}	4.24×10^{-5}	0.18	0.06
M-3	9.522×10^{-5}	2.96×10^{-5}	0.18	0.04
M-4	9.27×10^{-5}	2.34×10^{-5}	0.18	0.00

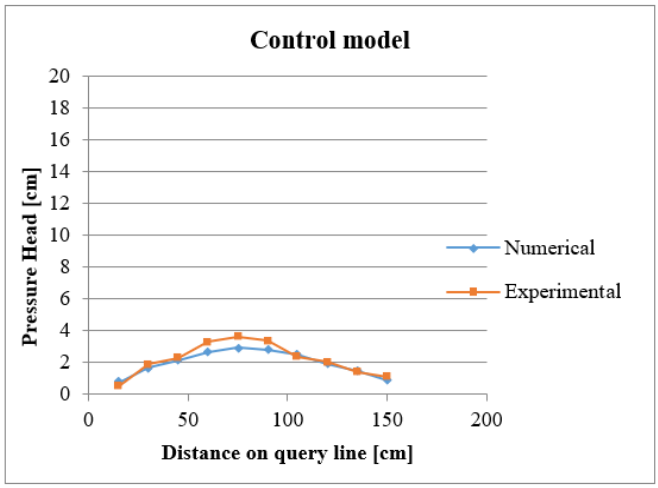

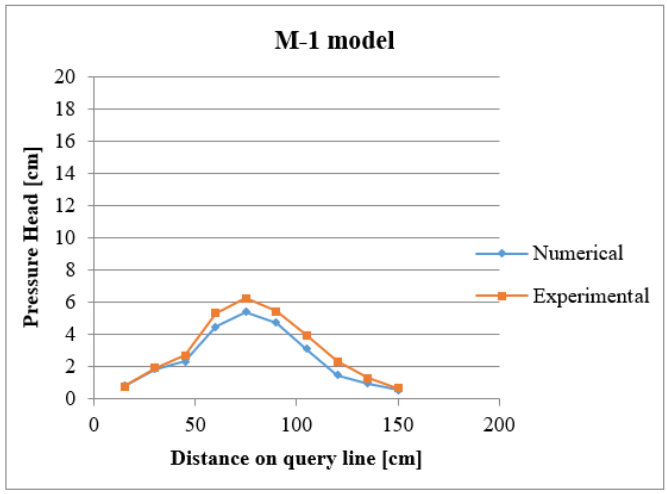

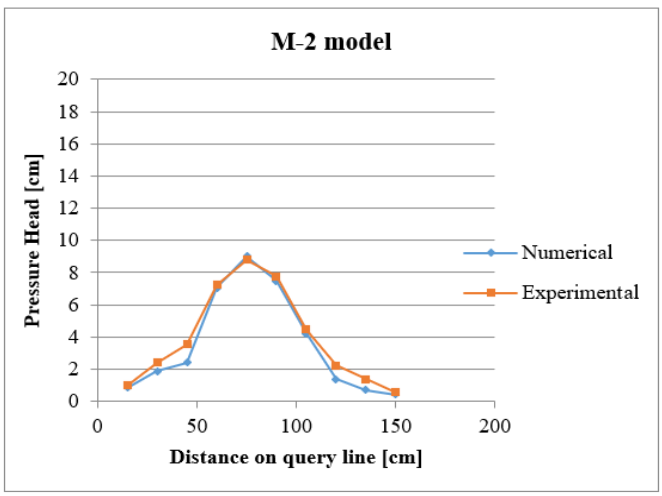

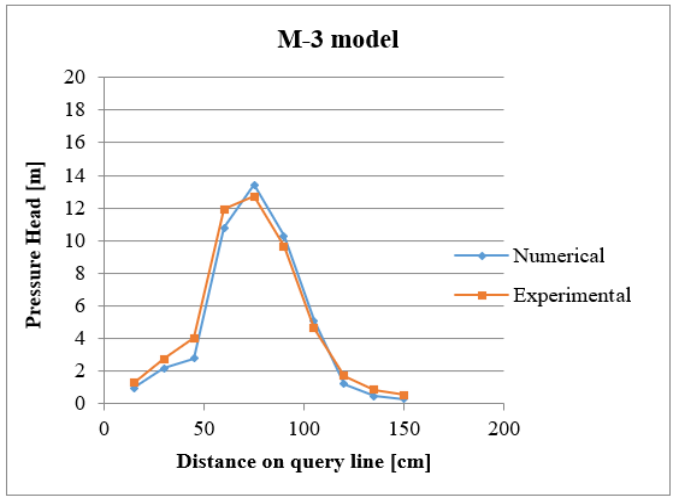

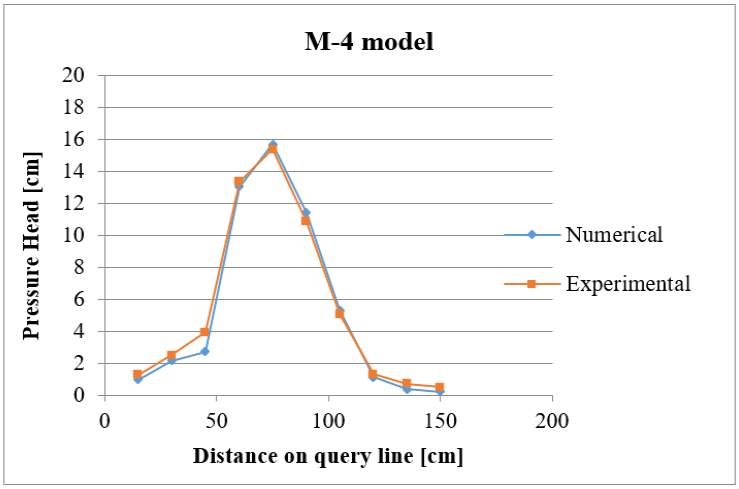

Figure 17. Comparison of the phreatic surface between numerical simulations and experimental measurements for both control and treated models at the 5 min stage of rapid drawdown

4. CONCLUSIONS

The experimental and numerical results demonstrated that lime–fly ash treatment significantly influenced pore water pressure dissipation in earth dams under rapid drawdown conditions by reducing core permeability and increasing the time required to reach hydraulic equilibrium. The untreated control model showed the fastest dissipation, with the pressure head stabilizing shortly after the 8 min mark. In contrast, the treated models exhibited progressively delayed dissipation, proportional to the additive content. Model M-4 exhibited the slowest dissipation and reached stabilization after nearly 45 min, indicating the most pronounced reduction in hydraulic conductivity among the tested mixtures. Despite the delayed dissipation in the treated cores, the high permeability of the shell zone consistently facilitated rapid pore pressure release, preventing adverse impacts on upstream slope stability.

Validation with numerical modeling confirmed the experimental measurements, showing excellent agreement in phreatic surface behavior. Downstream seepage decreased progressively with treatment, while exit gradients were effectively reduced to zero on the downstream slope at higher treatment levels. In general, lime–fly ash treatment significantly improved core impermeability and reduced seepage; however, excessive reductions in permeability prolonged excess pore pressures and increased the risk of hydraulic instability during rapid drawdown. High-permeability shell zones on the sides of the core zone were therefore essential to achieve a balance between permeability control and pore pressure dissipation.

While this study focused on the hydraulic behavior of earth dams under rapid drawdown and the effects of lime–fly ash treatment, future research is recommended to investigate slope stability under transient conditions, microstructural changes from soil treatment, and the evaluation of shear strength parameters to provide a more comprehensive understanding of treated dam performance.

REFERENCES

[1] Design Standards No. 13: Embankment Dams. Chapter 4 – Static Stability Analyses, 2011. U.S. Department of the Interior, Bureau of Reclamation, Denver, CO, USA.

[2] General design and construction considerations for earth and rock-fill dams. Engineer Manual EM 1110-2-2300, 2003. Department of the Army, Washington, DC, USA.

[3] Guardiani, C., Soranzo, E., Wu, W. (2022). Time-dependent reliability analysis of unsaturated slopes under rapid drawdown with intelligent surrogate models. Acta Geotechnica, 17(4): 1071-1096. https://doi.org/10.1007/s11440-021-01364-w

[4] Bijeljanin, L., Ferreira, N. (2008). Fluid reservoir slope instability due to drawdown effect. In Proceedings of the Canadian Geotechnical Society GEO-2008 Conference, pp. 1412-1417.

[5] Alonso, E.E., Pinyol, N.M. (2016). Numerical analysis of rapid drawdown: Applications in real cases. Water Science and Engineering, 9(3): 175-182. https://doi.org/10.1016/j.wse.2016.11.003

[6] Ahmed, T.M. (2025). Dynamic analysis of pore water pressure variation and stability in earth dams during rapid and slow drawdown: Khassa Chai Earth Dam as a case study. Eurasian Journal of Science and Engineering, 11(1): 11-23. https://doi.org/10.23918/eajse.v11i1p2

[7] Noori, K.M.G., Salim, S.G. (2021). The influence of shell permeability on stability of upstream slope during rapid drawdown – Khassa Chai Earth Dam as a case study. Iraqi National Journal of Earth Science, 21(2): 15-28. https://doi.org/10.33899/earth.2021.170383

[8] Pandey, B.R., Knoblauch, H., Zenz, G. (2023). Slope stability evaluation due to reservoir draw-down using LEM and stress-based FEM along with Mohr–Coulomb criteria. Water, 15(22): 4022. https://doi.org/10.3390/w15224022

[9] Terzaghi, K., Peck, R.B., Mesri, G. (1996). Soil Mechanics in Engineering Practice (3rd ed.). John Wiley and Sons, Inc., USA.

[10] Reddi, L.N. (2003). Seepage in Soils: Principles and Applications (1st ed.). John Wiley and Sons, Inc., USA.

[11] Abramson, L.W., Lee, T.S., Sharma, S., Boyce, G.M. (2002). Slope Stability and Stabilization Methods (2nd ed.). John Wiley and Sons, Inc., USA.

[12] Shuhaib, Z.K., Khassa, S.I. (2024). Influence of permeability anisotropy on seepage and slope stability of an earthen dam during rapid and slow drawdown.

Mathematical Modelling of Engineering Problems, 11(5): 1355-1365. https://doi.org/10.18280/mmep.110527
[13] Pakmanesh, M., Mousavi Jahromi, S., Khosrojerdi, A., Hassanpour Darvishi, H., Babazadeh, H. (2021). Experimental and numerical study of upstream slope stability in an earth dam reservoir under rapid drawdown conditions. Progress in Computational Fluid Dynamics, an International Journal, 21(4): 248-260. https://doi.org/10.1504/PCFD.2021.116521
[14] Kahot, Z. (2025). Numerical modeling of saturated – unsaturated seepage flow in porous media and slope stability analysis in an earth dam following rapid drawdown. Transylvanian Review. https://transylvanianreviewjournal.com/index.php/TR/article/view/1158.
[15] Soralump, S., Panthi, K., Prempramote, S. (2021). Assessment of the upstream slope failure of a dam due to repeated cyclic drawdown. Soils and Foundations, 61(5): 1386-1398. https://doi.org/10.1016/j.sandf.2021.08.006
[16] Mahmood, N.S., Aude, S.A., Abdullah, H.H., Sulaiman, S.O., Al-Ansari, N. (2022). Analysis of slope stability and soil liquefaction of zoned earth dams using numerical modeling. International Journal of Design and Nature and Ecodynamics, 17(4): 557-562. https://doi.org/10.18280/ijdne.170409
[17] Topçu, E., Bağrıaçık, B., Erdağ, A. (2022). Stability analysis of an embankment dam during rapid drawdown of water in reservoir. Journal of Engineering Sciences and Design, 10(1): 50-60. https://doi.org/10.21923/jesd.928763
[18] Charrak, H., Smail, N., Rouissat, B., Basri, H., Alsamawi, A.B. (2024). Analysis of upstream slope stability during rapid drawdown – Sidi Abdelli dam case study. Journal of Geomechanics and Geoengineering, 2: 1-6. https://doi.org/10.38208/jgg.v2.444
[19] Onyekwena, C.C., Liu, H. (2025). Stability analysis of geotextile reinforced unsaturated slope under drawdown conditions. Geosystems and Geoenvironment, 4(4): 100423. https://doi.org/10.1016/j.geogeo.2025.100423
[20] Taghvaei, P., Mousavi, S.F., Shahnazari, A., Karami, H., Shoshpash, I. (2019). Experimental and numerical modeling of nano-clay effect on seepage rate in earth dams. International Journal of Geosynthetics and Ground Engineering, 5(1): 1. https://doi.org/10.1007/s40891-018-0152-8
[21] Alzamily, Z.N., Sh. Abed, B. (2022). Experimental and theoretical investigations of seepage reduction through zoned earth dam material with special core. Materials Today: Proceedings, 61: 998-1005. https://doi.org/10.1016/j.matpr.2021.10.283
[22] Shuhaib, Z.K., Khassaf, S.I. (2023). Experimental and numerical evaluation of tire rubber powder effectiveness for reducing seepage rate in earth dams. Open Engineering, 13(1): 1-13. https://doi.org/10.1515/eng-2022-0422
[23] Arslan, E., Develioğlu, I., Pulat, H.F. (2025). A comparative study on the performance of freeze thaw cycled alluvial soils stabilized with lime and fly ash. Karadeniz Fen Bilimleri Dergisi, 15(3): 1094-1118. https://doi.org/10.31466/kfbd.1609555
[24] Sambre, T., Endait, M., Patil, S. (2024). Sustainable soil stabilization of expansive soil subgrades through lime fly ash admixture. Discover Civil Engineering, 1(1): 65. https://doi.org/10.1007/s44290-024-00063-1
[25] Arias Jaramillo, Y.P., Gómez Cano, D., Carvajal, G.I., Hidalgo, C.A., Muñoz, F. (2023). Evaluation of the effect of binary fly ash lime mixture on the bearing capacity of natural soils: A comparison with two conventional stabilizers lime and Portland cement. Materials, 16(11): 13996. https://doi.org/10.3390/ma16113996
[26] Husein, F., Chemeda, Y.C. (2018). Lime stabilization of highly plastic clayey soil for the impervious core of embankment dam: The case of Gidabo dam, Ethiopia. Ethiopian Journal of Science and Sustainable Development, 5(2): 27-40.
[27] Islam, M.S., Islam, T., Khatun, N. (2021). Permeability alteration of low plastic clay and poorly graded sand using lime and fly ash. Indian Geotechnical Journal, 51(5): 967-978. https://doi.org/10.1007/s40098-020-00493-5
[28] Swamynaidu, M., Tyagi, A. (2024). Hydraulic conductivity of cement and fly ash stabilised clay mixes – Application to soil mixing techniques for seepage barrier construction. Construction and Building Materials, 374: 136533. https://doi.org/10.1016/j.conbuildmat.2024.136533
[29] Design of Small Dams. (1987). U.S. Department of the Interior Bureau of Reclamation, USA.
[30] Iraqi Standard Specification. (2004). Lime That Used in Building, No. 807. https://www.alnoora-iraq.com/.
[31] ASTM C618-20. (2020). Standard specification for coal fly ash and raw or calcined natural pozzolan for use in concrete. ASTM International, West Conshohocken, PA, USA. https://doi.org/10.1520/C0618-22
[32] Das, B.M. (2011). Principles of Foundation Engineering. Cengage Learning, Stamford, CT, USA.
[33] Fang, H.Y. (1991). Foundation Engineering Handbook. Chapman and Hall, New York, USA.
[34] Arora, K.R. (1992). Soil Mechanics and Foundation Engineering in S.I. Units. Standard Publishers Distributors, New Delhi, India.
[35] Murthy, V.N.S. (2010). Advanced Foundation Engineering: Geotechnical Engineering Series. CBS Publishers and Distributors, New Delhi, India.
[36] ASTM D2434-19. (2019). Standard test method for permeability of granular soils (constant head), ASTM International, West Conshohocken, PA, USA. https://doi.org/10.1520/D2434-19
[37] ASTM D5084-16. (2016). Standard test methods for measurement of hydraulic conductivity of saturated porous materials using a flexible wall permeameter, ASTM International, West Conshohocken, PA, USA. https://doi.org/10.1520/D5084-16